Accurate determination of saturation parameters for Cr^{4+}-doped solid-state saturable absorbers

Alphan Sennaroglu, Umit Demirbas, Sarper Ozharar,* and Fatih Yaman†

Departments of Physics and Electrical–Electronics Engineering, Laser Research Laboratory, Koç University, Rumelifeneri, Sariyer, Istanbul 34450 Turkey

Received March 4, 2005; revised July 31, 2005; accepted September 7, 2005

We describe a systematic, rigorous procedure for the determination of the optical absorption saturation parameters for Cr^{4+}:YAG and Cr^{4+}:forsterite crystals at 1064 nm. A rate-equation approach was used to analyze the cw and pulsed transmission data of several crystals by accounting for the transverse as well as longitudinal variation of the beam intensity, saturation effects, and excited-state absorption. Use of an iterative procedure whereby the cw and pulsed data were simultaneously analyzed led to a considerable reduction in the error for the determination of cross sections. The average value of the absorption cross section σ_a and the normalized excited-state absorption cross section $f_p=\sigma_{esa}/\sigma_a$ were determined to be 6.13×10^{-19} cm^2 and 0.45, respectively, for Cr^{4+}:forsterite and 19.6×10^{-19} cm^2 and 0.06, respectively, for Cr^{4+}:YAG. Detailed comparison was also made with previous saturation measurements in the literature. Our results further show that lumped models based on the thin-length approximation should be used with caution in the determination of cross sections, especially when the pump beam is tightly focused inside the absorber.

OCIS codes: 140.3580, 160.6990.

1. INTRODUCTION

In addition to their use as tunable laser media in the near-infrared region,[1] Cr^{4+}-doped crystals such as Cr^{4+}:YAG and Cr^{4+}:forsterite have also been employed as saturable absorbers in passively Q-switched and–or mode-locked solid-state lasers near 1 μm,[2–7] owing to the presence of strong absorption bands in that region. Two important factors that influence the performance of these materials in passive Q switching are the strength of ground-state absorption and the existence of unwanted excited-state absorption, characterized by the cross sections σ_a and σ_{esa}, respectively. Because accurate determination of the cross sections is very important in the evaluation of passive Q switches, investigation of the saturation mechanism in these materials has attracted a great deal of attention over the past decade.[2,3,5,7–21] However, a large discrepancy still remains among the reported cross-section values of the Cr^{4+}-doped media, calling for a systematic procedure for the determination of the saturation parameters.

In this work, we present the results of a detailed investigation aimed at accurately determining the saturation parameters of Cr^{4+}:YAG and Cr^{4+}:forsterite saturable absorbers. A rate-equation analysis was employed to analyze the cw and pulsed transmission data of several samples. A four-level energy scheme was assumed, and effects due to saturation, excited-state absorption, and transverse intensity variations were taken into account. In the experiments, both cw and pulsed transmission data were collected at 1064 nm. Our results show that when cw and pulsed transmission data are analyzed separately, we see a large spread in the best-fit cross-section values. On the other hand, if cw and pulsed data are analyzed iteratively so that the small-signal absorption coefficient is determined from the cw data and the excited-state absorption cross section is determined from the pulsed data, a significant reduction in the spread of the cross-section values is observed.

The paper is organized as follows. Section 2 describes the rate-equation models that we used for the analysis of cw and pulsed transmission data. The experimental setup is described in Section 3. The analysis of the experimental data and the details of the iterative fitting procedure are further discussed in Section 4.A. The average best-fit values of σ_a and f_p ($f_p=\sigma_{esa}/\sigma_a$) were determined to be 6.13×10^{-19} cm^2 and 0.45, respectively, for Cr^{4+}:forsterite; in the case of Cr^{4+}:YAG, σ_a and f_p were 19.6×10^{-19} cm^2 and 0.06, respectively. In Section 4.B, we assess the validity of lumped saturation models and show that use of the thin-length approximation in the determination of cross sections leads to a large discrepancy in best-fit values. This was because the pump beam was tightly focused inside most of the absorbers considered in this study.

2. THEORY

A. Continuous-Wave Case

In this section, we derive the differential equations that govern the spatial evolution of the beam power or energy through the saturable absorber. Let us consider the energy-level diagram in Fig. 1 to model a saturable absorber subject to excited-state absorption. In the presence of pump photons at the wavelength of λ_p, absorber ions are first excited from the ground state $|g\rangle$ to the first excited-state $|3\rangle$ as a result of stimulated absorption. Fast nonradiative decay then occurs to the upper level $|2\rangle$. In the case of Cr^{4+}:forsterite and Cr^{4+}:YAG, level $|2\rangle$ serves also as the upper laser level from which ions may decay via stimulated or spontaneous emission to the lower level $|1\rangle$. In our analysis, we have neglected the stimulated

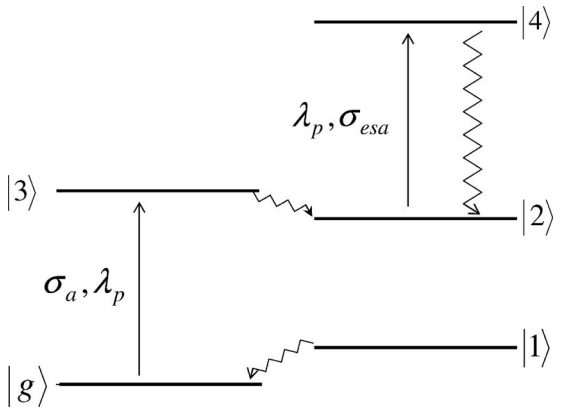

Fig. 1. Energy-level diagram of a saturable absorber exhibiting excited-state absorption. Zig-zagged lines indicate nonradiative decay processes.

emission processes. Fast nonradiative decay finally brings the ions from state $|1\rangle$ back to the ground state $|g\rangle$. Because nonradiative decay rates are very fast, in comparison with decay rates of level, populations of levels $|1\rangle$ and $|3\rangle$ are assumed to be negligible. Finally, we assume that excited-state absorption may also take place from level $|2\rangle$ to a higher-lying level $|4\rangle$ at the pump wavelength of λ_p and that ions excited to level $|4\rangle$ undergo a rapid nonradiative decay back to $|2\rangle$. The population densities $N_g(r,z)$ (ground state) and $N_2(r,z)$ (upper level) obey the following rate equations:

$$\frac{\partial N_2(r,z)}{\partial t} = -\frac{\partial N_g(r,z)}{\partial t} = \frac{\sigma_a \lambda_p I_p(r,z)}{hc} N_g(r,z) - \frac{N_2(r,z)}{\tau_f}, \tag{1}$$

where h is Planck's constant, c is the speed of light, $I_p(r,z)$ is the intensity of the pump radiation at λ_p, σ_a is the ground-state absorption cross section at λ_p, and τ_f is the fluorescence lifetime. The quantity $(\sigma_a \lambda_p I_p N_g / hc)$ gives the number of atoms per unit volume per unit time undergoing stimulated absorption. In the following analysis, we will drop the spatial dependence of the intensities and population densities.

We next consider a thin slab of the saturable absorber to derive the differential equation satisfied by the pump intensity. The thickness and the cross-sectional area of the slab are taken to be dz and A, respectively. Conservation of energy gives

$$A\mathrm{d}z \frac{\partial u_p}{\partial t} = [I_p(z) - I_p(z+\mathrm{d}z)]A - (N_g \sigma_a I_p + N_2 \sigma_{esa} I_p) A \mathrm{d}z, \tag{2}$$

where u_p is the electromagnetic energy density at the wavelength λ_p and $(N_g \sigma_a I_p + N_2 \sigma_{esa} I_p)$ corresponds to the pump energy lost per unit volume per unit time owing to ground-state and excited-state absorption. Here, σ_{esa} is the excited-state absorption cross section. Simplifying and by using the relation $u_p = v_g I_p$ (v_g = group velocity), we obtain

$$\frac{\partial I_p}{\partial z} + \frac{1}{v_g}\frac{\partial I_p}{\partial t} = -\sigma_a I_p (N_g + f_p N_2). \tag{3}$$

In Eq. (3), f_p is the normalized strength of the excited-state absorption at λ_p, defined according to

$$f_p = \frac{\sigma_{esa}(\lambda_p)}{\sigma_a(\lambda_p)}. \tag{4}$$

For the cw case, we concentrate on the steady-state solution of Eqs. (1) and (2). Noting that $N_2 + N_g = N_T$, where N_T is the total ion density, the steady-state expression for N_2 becomes

$$N_2 = N_T \frac{I_p / I_{sa}}{1 + I_p / I_{sa}}. \tag{5}$$

Here, I_{sa} ($I_{sa} = hc/\sigma_a \lambda_p \tau_f$) is the absorption saturation intensity. By using the steady-state expressions for N_2 and N_g, the differential equation describing the spatial evolution of the pump intensity can be written as

$$\frac{\partial I_p}{\partial z} = -\alpha_{p0} I_p \left(\frac{1 + f_p \dfrac{I_p}{I_{sa}}}{1 + \dfrac{I_p}{I_{sa}}} \right). \tag{6}$$

In Eq. (6), α_{p0} ($\alpha_{p0} = N_T \sigma_a$) is the small-signal differential pump-absorption coefficient.

To derive the differential equation satisfied by the beam power, we assume that the pump intensity (I_p) has a transverse distribution given by

$$I_p(r,z) = P_p(z) \Phi_p(r,z), \tag{7}$$

where $P_p(z)$ is the pump power at the location z and r is the radial coordinate. The normalized distribution function Φ_P is assumed to be Gaussian:

$$\Phi_P = \frac{2}{\pi \omega_p^2} \exp\left(-\frac{2r^2}{\omega_p^2} \right). \tag{8}$$

Above, ω_p is the position-dependent pump spot-size function. By integrating Eq. (6) over the beam cross section and by using Eqs. (7) and (8), we obtain

$$\frac{\mathrm{d}P_p}{\mathrm{d}z} = -\alpha_{p0} P_p \int_0^\infty \mathrm{d}r 2\pi r \Phi_p \left(\frac{1 + f_p \dfrac{P_p \Phi_p}{I_{sa}}}{1 + \dfrac{P_p \Phi_p}{I_{sa}}} \right). \tag{9}$$

Note from Eq. (9) that in the limit as I_{sa} goes to infinity, the pump power P_p decays exponentially inside the saturable absorber as expected.

B. Pulsed Case

We next consider the case in which a periodic pulse train is incident on the saturable absorber. The pulse intensity $I_p(t)$ and the integrated energy density $\bar{E}_p$ are related through

$$\int_{-\infty}^{\tau} dt I_p(t) = \bar{E}_p, \tag{10}$$

where τ is much greater than the pulsewidth so that $I_p(\tau)$ is essentially 0. By using Eq. (1), Eq. (3) can be recast into the form

$$\frac{\partial I_p}{\partial z} + \frac{1}{v_g}\frac{\partial I_p}{\partial t} = (1-f_p)\frac{hc}{\lambda_p}\frac{\partial N_g}{\partial t} - f_p \alpha_{p0} I_p. \tag{11}$$

Integrating Eq. (1) from $t=-\infty$ to $t=\tau$ with the initial condition $N_g(-\infty)=N_T=\alpha_{p0}/\sigma_a$, and with the assumption that τ is much shorter than the fluorescence lifetime τ_f leads to

$$N_g = N_T \exp\left(-\frac{\bar{E}_p}{E_{sa}}\right), \tag{12}$$

where E_{sa} ($E_{sa}=hc/\sigma_a\lambda_p$) is the absorption saturation fluence. Next, we integrate Eq. (11) from $t=-\infty$ to $t=\tau$ and use Eq. (12) to obtain the differential equation satisfied by the pump energy density:

$$\frac{\partial \bar{E}_p}{\partial z} = -(1-f_p)\alpha_{p0}E_{sa}\left[1-\exp\left(-\frac{\bar{E}_p}{E_{sa}}\right)\right] - f_p\alpha_{p0}\bar{E}_p. \tag{13}$$

Similar to the continuous-wave case, we assume that the pulse energy density and the total energy E_p per pulse are related according to

$$\bar{E}_p = E_p \Phi_p, \tag{14}$$

where Φ_p is given by Eq. (8). Integrating over the beam cross-section, we obtain

$$\frac{\partial E_p}{\partial z} = -(1-f_p)\alpha_{p0}E_{sa}\int_0^{\infty} dr 2\pi r\left[1-\exp\left(-\frac{E_p\Phi_p}{E_{sa}}\right)\right] - f_p\alpha_{p0}E_p. \tag{15}$$

Note that if the pulse repetition rate of the pulsed laser is f_0, then the average incident power P_i and the incident energy E_{pi} per pulse are related through $f_0E_{pi}=P_i$. Equations (9) and (15) were used to analyze the cw and pulsed transmission data of the Cr^{4+}:YAG and Cr^{4+}:forsterite samples.

3. EXPERIMENT

The experimental setup is shown in Fig. 2. The cw and pulsed transmission data of the Cr^{4+}:forsterite and Cr^{4+}:YAG samples were measured by using a 1064 nm flashlamp-pumped Nd:YAG laser (Quantronix, Model 116) that could be operated in cw or *Q*-switched mode. In

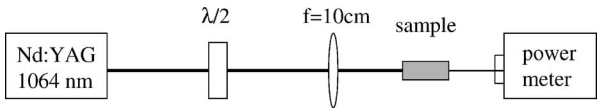

Fig. 2. Sketch of the experimental setup (λ/2, half-wave plate at 1064 nm).

Table 1. Length and Small-Signal Absorption Coefficient α_{p0} of Each Sample Used in the Saturation Measurements[a]

Sample	Sample Number	Length (mm)	α_{p0} (cm^{-1})	Beam Waist (μm)
Cr^{4+}:forsterite	1	20	1.63	25
Cr^{4+}:forsterite	2	20	0.60	25
Cr^{4+}:forsterite	3	20	1.51	25
Cr^{4+}:YAG	1	20	1.11	25
Cr^{4+}:YAG	2	20	1.09	25
Cr^{4+}:YAG	3	1.56	1.45	100
Cr^{4+}:YAG	4	0.72	2.00	100

[a]The measured beam waist is also shown for each sample.

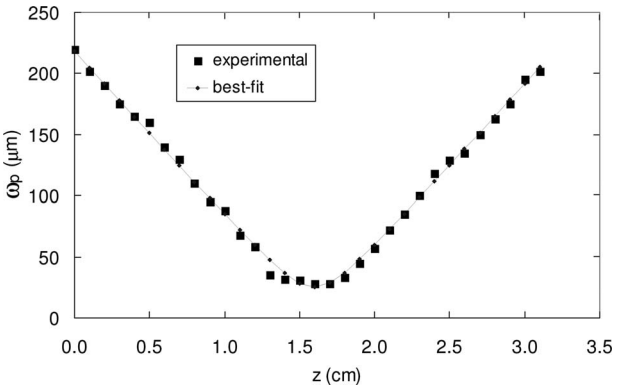

Fig. 3. Measured and fit variations of the spot-size function $\omega_p(z)$ as a function of position z. The best-fit values of the beam waist and the M^2 factor were determined to be 25 μm and 1.04, respectively.

Q-switched mode, the laser produced 140 ns pulses at a 1 kHz repetition rate. Table 1 lists the dimensions and the small-signal absorption coefficient of the samples used in the experiments. Except for the two thin antireflection-coated Cr^{4+}:YAG samples (Cr^{4+}:YAG Samples 3 and 4 in Table 1), all the other crystals were Brewster cut. With the half-wave plate (λ/2 in Fig. 2), the pump-beam polarization was adjusted to minimize the Fresnel losses, which could be kept below 0.2%. All measurements were performed at room temperature. The pump beam was focused with a lens having a 10 cm focal length, and the transmitted power was measured with a power meter (Molectron, Model 5100). In the case of pulsed pumping, the average transmitted power was measured with the same power meter, and the corresponding transmitted energy was determined by diving the average power by the pulse-repetition rate (1 kHz in this case). The measured variation of the pump spot-size function $\omega_p(z)$ with relative position is shown in Fig. 3. Spot-size measurements were performed by using the knife-edge technique. In particular, a sharp, vertical razor blade was scanned across the beam cross section to determine the transverse locations x_1 and x_2 which gave 84% and 16% power transmission, respectively. The spot-size at that location is then given by $|x_2-x_1|$.To determine the beam parameters, $\omega_p(z)$ was assumed to have the functional form

$$\omega_p(z) = \omega_{p0}\left[1 + \left(\frac{z - z_{fp}}{z_{Rp}}\right)^2\right]^{1/2}, \tag{16}$$

where ω_{p0} is the pump beam waist, z_{fp} is the beam-waist location, and z_{Rp} ($z_{Rp}=n_0\pi\omega_{p0}^2/M^2\lambda_p$, n_0, refractive index of the crystal; and M^2, beam-quality factor) is the Rayleigh range. For this beam geometry, the best-fit values of M^2 and ω_{p0} were determined to be 1.04 and 25 μm, respectively. In the case of the thin Cr^{4+}:YAG samples, we used a less tightly focused beam with a measured waist of 100 μm (Cr^{4+}:YAG samples 3 and 4 in Table 1).

4. RESULTS AND DISCUSSION

A. Cross-Section Values for Cr^{4+}:Forsterite and Cr^{4+}:YAG

Equations (9) and (15) can be used to investigate the dependence of the transmission on the key parameters of the saturable absorber for the cw and pulsed cases. As an example, consider Figs. 4(a) and 4(b) which show how the transmission varies as a function of the incident pump power and the incident pulse energy for the cw and pulsed cases, respectively, for a hypothetical saturable absorber ($\sigma_a=25\times10^{-19}$ cm^2, $\tau_f=5$ μs, $\alpha_{p0}=1.5$ cm^{-1}, $\lambda_p=1064$ nm, $L_0=20$ mm, $n_0=1.635$, $z_{fp}=L_0/2$, and$\omega_{p0}=25$ μm). Here, L_0 is the crystal length. Calculations were done for different values of f_p. Note that in each case, the maximum

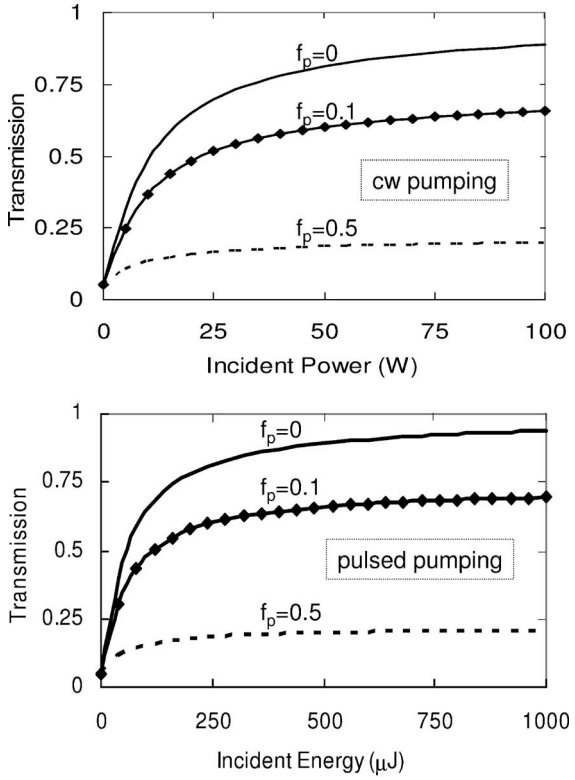

Fig. 4. Calculated variation of the transmission for a hypothetical absorber as a function of (a) incident power (cw case) and (b) incident pulse energy (pulsed case) for different amounts of excited-state absorption. (Absorber parameters: $\sigma_a=25\times10^{-19}$ cm^2, $\tau_f=5$ μs, $\alpha_{p0}=1.5$ cm^{-1}, $\lambda_p=1064$ nm, $L_0=20$ mm, $n_0=1.635$, $z_{fp}=L_0/2$, $\omega_{p0}=25$ μm).

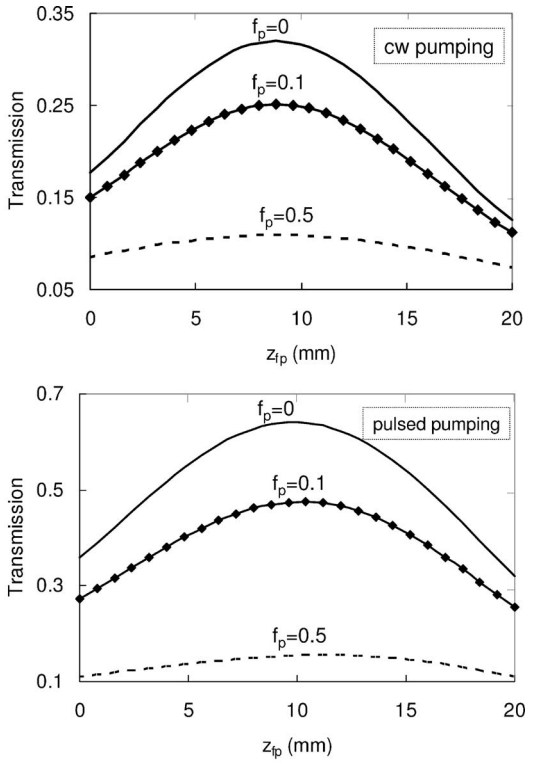

Fig. 5. Calculated variation of the transmission for a hypothetical absorber as a function of the beam-waist location for the (a) cw and (b) pulsed cases for different levels of excited-state absorption. (Absorber parameters: $\sigma_a=25\times10^{-19}$ cm^2, $\tau_f=5$ μs, $\alpha_{p0}=1.5$ cm^{-1}, $\lambda_p=1064$ nm, $L_0=20$ mm, $n_0=1.635$, and $\omega_{p0}=25$ μm.)

transmission T_{max} obtained at very high intensities is limited by the presence of excited-state absorption and is given asymptotically by

$$T_{max} = \exp(-f_p\alpha_{p0}L_0). \tag{17}$$

Figures 5(a) and 5(b) show the calculated variation of the transmission as a function of the beam-waist location (z_{fp}) for the cw and pulsed cases. Here, the fixed parameters of the saturable absorber were $\sigma_a=25\times10^{-19}$ cm^2, $\tau_f=5$ μs, $\alpha_{p0}=1.5$ cm^{-1}, $\lambda_p=1064$ nm, $L_0=20$ mm, $n_0=1.635$, and $\omega_{p0}=25$ μm. In Fig. 5(a), the incident pump power was kept at 5 W, whereas the incident pump energy was 50 μJ in Fig. 5(b). Note that the transmission has a strong dependence on the beam-waist location and peaks when the beam is focused near the center of the crystal. This suggests that z-scan methods can also be employed to determine the value of the absorption cross section, as was done in previous studies.[13,18]

In our experiments, the samples were translated at a fixed incident pump power until the transmission was maximized, and then the variation of the transmission was measured as a function of the incident pump power or energy at this location. Two different approaches were used to determine the best-fit values of the cross sections. In the first case, the cw and pulsed transmission data of each sample were analyzed separately. Specifically, for a given set of $(\alpha_{p0},\sigma_a,f_p)$ trial values, the particular z_{fp} that maximizes the transmission was first determined, and the corresponding deviation between the measured and the calculated transmissions was calculated. The param-

eters α_{p0}, σ_a, and f_p were then varied to find the best-fit values that minimize the deviation. In principle, α_{p0} can also be measured accurately with a spectrophotometer to eliminate one of the unknown parameters. In this study, we chose to determine it by using the scheme described above, for two reasons. First, the procedure proposed in this paper requires no additional instrumentation other than the transmission measurement setup discussed in Section 3. Second, all of the 20 mm long samples used in our measurements (see Table 1) were Brewster cut, and this makes spectrum measurements with a spectrophotometer cumbersome.

The three Cr^{4+}:forsterite samples shown in Table 1 were first analyzed by use of the algorithm described above. The fluorescence lifetime τ_f and the crystal refractive index n_0 were taken to be 2.9 μs and 1.635, respectively.[21] In the measurements, the electric field was kept parallel to the b axis of the crystals ($E \| b$). The results, which are displayed in Table 2, show a large spread in the best-fit values. In particular, the fractional spread, defined as the ratio of the standard deviation to the average value, came to 1.16 and 0.28 for σ_a and f_p, respectively. These numbers were determined by considering the pulsed and cw transmission results of the three samples. The reason for the large variation in the best-fit values is that cw data alone do not reveal the behavior of the saturable absorbers in the high-intensity limit, hence making the accurate determination of f_p very difficult. Similarly, owing to small signal-to-noise ratio at low power levels, determination of α_{p0} is very sensitive to fluctuations in the case of pulsed transmission data.

We resolved this problem by using a second, iterative approach to determine the parameters of the saturable absorber. The steps of the analysis may be summarized as follows. The cw transmission data of each sample were first analyzed to determine the best-fit values of α_{p0}, σ_a, and f_p. The α_{p0} value determined from the cw data was kept fixed in the analysis of the pulsed data, and only σ_a and f_p were varied to determine the best-fit values. Next, the cw data were analyzed once again to determine σ_a. Here, the best-fit f_p value obtained from the analysis of the pulsed data and the best-fit α_{p0} value from the original cw analysis were kept fixed. The best-fit values of the saturation parameters for Cr^{4+}:forsterite obtained by using this scheme are shown in Table 3. Note that the use of the iterative procedure leads to a large reduction in the spread of the best-fit values. For example, the fractional spread was reduced from 1.16 to 0.25 and from 0.28 to 0.01 for the best-fit values of σ_a and f_p, respectively. Figures 6(a) and 6(b) show the resulting measured and fit variation of the transmission as a function of the incident

Table 2. Best-Fit Values of α_{p0}, f_p, and σ_a Obtained by Analyzing the cw and Pulsed Transmission Data of the Cr^{4+}:Forsterite Samples Separately

Sample No	α_{p0} (cm^{-1})		f_p		σ_a ($\times 10^{-19}$ cm^2)	
	cw	Pulsed	cw	Pulsed	cw	Pulsed
1	1.63	2.09	0.63	0.38	11.4	13.7
2	0.60	0.71	0.56	0.40	9.5	9.7
3	1.55	1.66	0.74	0.42	67.0	8.5

Table 3. Best-Fit Values of α_{p0}, f_p, and σ_a for Cr^{4+}:Forsterite Samples Obtained by Using the Iterative Analysis Scheme[a]

Sample Number	α_{p0} (cm^{-1})	f_p	σ_a ($\times 10^{-19}$ cm^2)	
			cw	Pulsed
1	1.63	0.46	6.3	5.1
2	0.60	0.45	6.5	4.3
3	1.51	0.45	8.8	5.8

[a]The average values of f_p and σ_a are 0.45 and 6.13×10^{-19} cm^2, respectively.

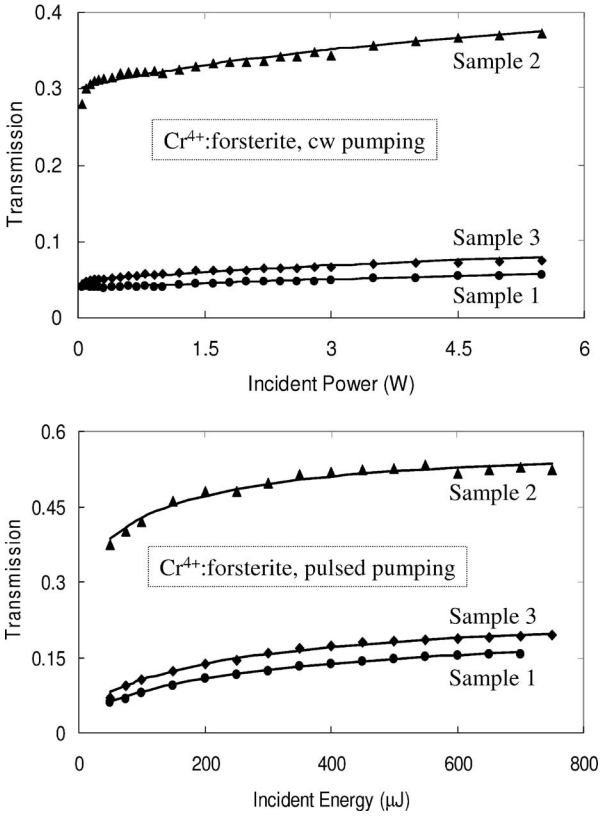

Fig. 6. Measured and fit variations of the transmission as a function of the (a) incident power (cw case) and (b) incident pulse energy (pulsed case) for the three Cr^{4+}:forsterite crystals.

Table 4. Previously Reported σ_a and f_p Values for Cr^{4+}:Forsterite in the Literature[a]

σ_a ($\times 10^{-19}$ cm^2)	f_p	Reference
1.36	0.13	23
6	0.48	16
23	—	2
1.9	—	17
1.9	—	9
2.5	0.3	8
6.11	0.31	Average
6.13[a]	0.45	This paper

[a]If more than one sample was used, only the average value is given.

Table 5. Best-Fit Values of α_{p0}, f_p, and σ_a Obtained by Analyzing the cw and Pulsed Transmission Data of the Cr^{4+}:YAG Samples Separately[a]

Sample Number	Orientation	α_{p0} (cm^{-1})		f_p		σ_a ($\times 10^{-19}$ cm^2)	
		cw	Pulsed	cw	Pulsed	cw	Pulsed
1	$E\|\|\langle 1,0,0\rangle$	1.11	0.63	0.07	0.10	26.2	8.1
2	$E\|\|\langle 1,0,0\rangle$	1.06	0.87	0.01	0.08	14.2	14.9
3	P1[a]	1.59	1.11	0.37	0.00	103.3	8.3
	P2[a]	1.58	0.96	0.58	0.00	152.2	5.8
4	P1[a]	1.99	1.37	0.04	0.00	23.5	5.1
	P2[a]	1.99	1.83	0.00	0.00	23.1	8.9

[a]P1 and P2 refer to the two orthogonal electric field polarizations used in the transmission measurements for samples 3 and 4 (See the text).

Table 6. Best-Fit Values of α_{p0}, f_p, and σ_a for Cr^{4+}:YAG Samples Obtained by Using the Iterative Analysis Scheme[a]

Sample Number	Orientation	α_{p0} (cm^{-1})	f_p	σ_a ($\times 10^{-19}$ cm^2)	
				cw	Pulsed
1	$E\|\|\langle 1,0,0\rangle$	1.11	0.06	25.7	20.4
2	$E\|\|\langle 1,0,0\rangle$	1.09	0.10	20.4	11.0
3	P1	1.42	0.02	24.5	15.0
	P2	1.47	0.10	17.4	24.0
4	P1	1.99	0.05	24.0	15.1
	P2	2.00	0.03	25.0	12.8

[a]The average values of f_p and σ_a are 0.06 and 19.6×10^{-19} cm^2, respectively.

power or pulse energy for the Cr^{4+}:forsterite samples. Here, the best-fit values obtained by using the iterative procedure were used. Table 4 lists some of the reported cross-section values in the literature for Cr^{4+}:forsterite. The average σ_a and f_p values of 6.13×10^{-19} cm^2 and 0.45 determined for Cr^{4+}:forsterite ($E\|b$) agree well with the average of the previously measured values and come closest to those reported by Kuleshov *et al.*[16]

A similar analysis was carried out with Cr^{4+}:YAG samples. In the calculations, the fluorescence lifetime τ_f and the crystal refractive index n_0 were taken to be 4.5 μs and 1.82, respectively.[21] Samples 1 and 2 shown in Table 1 were Brewster cut, and transmission measurements were performed by aligning the pump electric field along the <1,0,0> direction. Samples 3 and 4 were normal cut along the <0,0,1> direction. Since the complete orientation of each of these samples was not known, two sets of data were taken for each sample by aligning the electric field along two orthogonal directions. The results obtained for these polarizations are indicated as P1 and P2 in Tables 5 and 6. All of the measurements were averaged to determine the saturation parameters. Similar results were obtained as in the case of Cr^{4+}:forsterite. Whereas separate analysis of the cw and pulsed data gave larger deviations in the cross-section values, use of the iterative procedure again led to a reduction in the fractional spread of the best-fit values from 1.41 to 0.26 and from 1.76 to 0.56 for σ_a and f_p, respectively. Measured and fit values of transmission as a function of input power or pulse energy are displayed in Figs. 7(a) and 7(b). Finally, we compare the cross-section values determined in this study with previous reports. As can be seen from Table 7, the average σ_a value of 19.6×10^{-19} cm^2 determined in this study is close to the average of the previously reported values (23.3×10^{-19} cm^2). The average f_p value of the present study (0.06) is somewhat lower than the previous results (the average value in Table 7 is 0.16). Finally, since samples 3 and 4 were normal cut, we also compared the best α_{p0} values with those obtained from absorption spectrum measurements with a spectrophotometer. The aver-

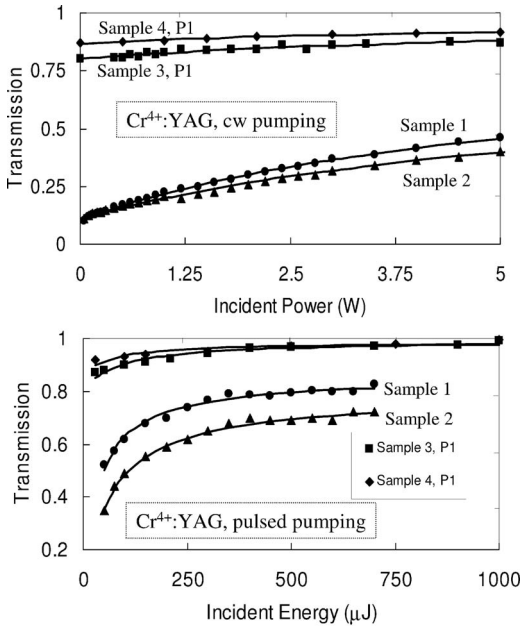

Fig. 7. Measured and fit variation of the transmission as a function of the (a) incident power (cw case) and (b) incident pulse energy (pulsed case) for the Cr^{4+}:YAG crystals.

Table 7. Previously Reported σ_a and f_p Values for Cr^{4+}:YAG in the Literature[a]

σ_a ($\times 10^{-19}$ cm^2)	f_p	Reference
23.2[a]	<0.06	20
5.8	—	13
70	0.29	15
13	—	12
16.4[a]	0.29	18
8.7	0.25	5
57	0.14	3
11.2	0.01	21
30	0.07	10
14	0.09	19
14.1[a]	0.12	24
3.6	—	25
50	0.09	26
—	0.4	27
32	0.14	7
8.7	0.25	28
15	0.07	29
23.29	0.16	Average
19.6[a]	0.06	This paper

[a]If more than one sample was used, only the average value is given.

age best-fit values for α_{p0} were 1.45 cm^{-1} and 2.00 cm^{-1} for samples 3 and 4, respectively, in good agreement with 1.54 and 1.95 cm^{-1} determined from spectrophotometer measurements.

Because the absorbed pump power could lead to lensing and modify the spot-size distribution inside the saturable absorber, we also investigated the effect of thermal lensing on cross-section measurements. The variation of the pump beam parameter $q(z)$ due to thermal lensing effects can be calculated by solving the differential equation

$$\frac{1}{q(z)^2} + \frac{d}{dz}\left(\frac{1}{q(z)}\right) + \beta(z)^2 = 0, \tag{18}$$

where $\beta(z)$ is the quadratic variation in the refractive index along the radial direction and is given by[22]

$$\beta(z) = \left[\frac{n_T h_0(z)}{2\kappa n_0}\right]^{1/2}. \tag{19}$$

Here, $n_T = dn/dT$ is the thermal index coefficient, κ is the heat conductivity, n_0 is the refractive index, and $h_0(z)$ is the axial value of the pump-induced heat deposition rate per unit volume given by

$$h_0(z) = \frac{\alpha_{p0}}{1 + (I_p/I_{sa})}\eta_h I_p. \tag{20}$$

The heating fraction η_h appearing in Eq. (20) is close to unity for both Cr^{4+}:forsterite and Cr^{4+}:YAG.[21] In the absence of thermal lensing, $\beta(z) = 0$ in Eq. (18), and one recovers the well-known solutions of Gaussian beam propagation in a homogeneous medium. First, we investigated the effect of cw thermal lensing in Cr^{4+}:forsterite ($n_T = 2.2 \times 10^{-6}$/K, $\kappa = 5$ W/m/K, $\eta_h = 0.91$). For each sample, the best-fit values of α_{p0} and f_p were kept fixed, and the change in the best-fit value of σ_a was calculated in the presence of thermal lensing. The average fractional change in the best-fit σ_a values came to 6.2%. In the case of Cr^{4+}:YAG ($n_T = 9.8 \times 10^{-6}$/K, $\kappa = 12$ W/m/K, $\eta_h = 0.93$), the corresponding variation in the best-fit value of σ_a was less than 1%, owing to the stronger influence of saturation at high pumping levels [see Eq. (20) above for the axial heat source h]. Because the estimated fractional changes in σ_a were small, the influence of thermal lensing was neglected in our analysis. As discussed below, neglect of thermal lensing was also taken into account in order to determine the overall measurement errors.

The error in absorption cross-section values was determined for both Cr^{4+}:forsterite and Cr^{4+}:YAG. In the experiments, errors in transmission and spot-size measurements were estimated to be ±1% and ±6%, respectively. For each sample, the best-fit f_p and α_{p0} values were kept fixed, and the resulting error in the best-fit σ_a values was calculated. For Cr^{4+}:forsterite, the overall average error due to measurement uncertainties and the neglect of thermal lensing was estimated to be ±6.4%. In the case of Cr^{4+}:YAG, the corresponding error was ±12%.

B. Validity of Lumped Models

An alternative analysis of saturable absorbers involves the use of lumped models in which the absorber is treated as a thin medium. In this section, we follow this approach to investigate the saturation behavior of the samples. Best-fit saturation parameters of the lumped model are determined and compared with those of the distributed models (Sections 2.A and 2.B) to assess the validity of the thin-length approximation.

When the transverse and longitudinal variation of the beam inside the sample is neglected, the cw transmission T_{cw} of the saturable absorber subject to excited-state absorption can be calculated from

$$T_{cw} = 1 - q_0 \frac{1 + f_p(P_p/P_{sa})}{1 + (P_p/P_{sa})}, \tag{21}$$

where q_0 is the small-signal absorption ($q_0 = \alpha_{p0}L_0$; L_0 is the crystal length), P_p is the incident pump power, and P_{sa} is the saturation power ($P_{sa} = I_{sa}A_{eff}$, A_{eff} is the effective cross-sectional area of the beam). Equation (21) can be readily derived by using the rate-equation approach of Section 2 along with the "thin-length" and plane-wave approximations. For the pulsed case, the transmission T_{pulsed} becomes

$$T_{pulsed} = 1 - q_0 \frac{(1 - f_p)}{E_p/E_A}[1 - \exp(-E_p/E_A)] - q_0 f_p. \tag{22}$$

In Eq. (22), E_p is the incident energy per pulse and E_A is the saturation energy ($E_A = E_{sa}A_{eff}$). Note that as the pulse energy E_p in Eq. (22) tends to zero, the small-signal transmission becomes 1-q_0, as expected. All of the

Table 8. Best-Fit Values of f_p, q_0, P_{sa}, and σ_a for the cw Transmission Data of Cr^{4+}:YAG and Cr^{4+}:Forsterite Samples Obtained with the Lumped Models

Material	Sample	f_p	q_0	P_{sa} (W)	σ_a ($\times 10^{-19}$ cm^2)
Cr^{4+}:YAG	1	0.15	0.89	5.8	4.7
	2	0.07	0.88	9.6	2.8
	3, P1	0.46	0.22	1.6	68.5
	3, P2	0.64	0.22	1.1	99.7
	4, P1	0.18	0.13	5.6	19.6
	4, P2	0.06	0.13	6.6	16.6
Cr^{4+}:forsterite	1	0.85	0.96	39.1	1.1
	2	0.79	0.70	5.9	7.5
	3	0.96	0.95	2.5	17.7

Table 9. Best-Fit Values of f_p, q_0, P_s, and σ_a for the Pulsed Transmission Data of Cr^{4+}:YAG and Cr^{4+}:Forsterite Samples Obtained with the Lumped Models

Material	Sample	f_p	q_0	E_A (μJ)	σ_a ($\times 10^{-19}$ cm^2)
Cr^{4+}:YAG	1	0.22	0.65	58	2.5
	2	0.27	0.86	53	2.7
	3, P1	0.00	0.15	126	4.7
	3, P2	0.07	0.13	135	4.4
	4, P1	0.00	0.10	145	4.1
	4, P2	0.00	0.07	160	3.7
Cr^{4+}:forsterite	1	0.84	0.96	141	1.2
	2	0.63	0.71	60	2.9
	3	0.81	0.96	107	1.6

Cr^{4+}:forsterite and Cr^{4+}:YAG samples were also analyzed by using Eqs. (21) and (22) to determine the best-fit values of the parameters q_0, P_{sa}, E_A, and f_p. The results are shown in Tables 8 and 9 for the cw and pulsed cases, respectively. Note that the σ_a values shown in the last column of Tables 8 and 9 were determined by taking $A_{eff} = \pi\omega_{rms}^2$ where ω_{rms} is the minimum rms radius of the beam inside the sample. As can be seen from Tables 8 and 9, there is a large discrepancy in the results of the lumped models. In particular, the lumped models predict a larger amount of excited-state absorption in relation to the distributed models of Sections 2.A and 2.B. For example, in the case of Cr^{4+}:YAG, the average f_p comes 0.18, approximately 3 times larger than that determined by using the distributed models (See Tables 6 and 9). In the case of σ_a, both models predict approximately the same average best-fit value (19.6×10^{-19} cm^2 in the distributed model, as opposed to 19.5×10^{-19} cm^2 in the lumped model for Cr^{4+}:YAG). However, the fractional spread increased considerably in the case of the lumped model (0.26 for the distributed model in comparison with 1.61 for the lumped model in the case of Cr^{4+}:YAG). Similar results were obtained for Cr^{4+}:forsterite. Hence, we conclude from this comparison that lumped models cannot be used to make accurate predictions of the saturation parameters in our case. This is attributed to the large variation of the pump-beam spot size inside the samples due to tight focusing.

5. CONCLUSIONS

In this paper, we have provided a detailed investigation of the saturation behavior of Cr^{4+}:YAG and Cr^{4+}:forsterite crystals. A rate-equation approach was used to analyze several samples with a distributed model that accounts for the transverse as well as the longitudinal variation of the beam intensity inside the saturable absorber. An iterative procedure was used to analyze the cw and the pulsed transmission data simultaneously. This led to a dramatic reduction in the spread of the best-fit cross-section values for both absorbers. The obtained results are close to the average of the previously reported values for both Cr^{4+}:YAG and Cr^{4+}:forsterite. Comparing the saturation parameters for the two media, we find that the ground-state absorption cross section is approximately three times larger in Cr^{4+}:YAG than in Cr^{4+}:forsterite. Also, the strength of excited-state absorption was found to be significantly lower in the case of Cr^{4+}:YAG in comparison with Cr^{4+}:forsterite. Both of these characteristics make Cr^{4+}:YAG a more suitable passive Q switch for 1 μm lasers. Finally, the results of Section 4.B showed that in the analysis of saturable absorbers, lumped models based on the thin-length approximation should be used with caution, especially when the pump beam is tightly focused inside the samples.

ACKNOWLEDGMENTS

The authors thank Adnan Kurt and Ahmet Unal for help in the experiments. A. Sennaroglu also acknowledges the support of the Turkish Academy of Sciences in the framework of the Young Scientist Award Program AS/TUBA-GEBIP/2001-1-11. A. Sennaroglu is the corresponding author and can be reached by telephone at (90) 212 338 1429, by fax at (90) 212 338-1559, or by e-mail at asennar@ku.edu.tr.

*Present address, Center for Research and Education in Optics and Lasers, University of Central Florida, Orlando, Florida 32816-2700.

†Present address, Institute of Optics, University of Rochester, Rochester, New York 14627.

REFERENCES

1. A. Sennaroglu, "Broadly tunable Cr^{4+}-doped solid-state lasers in the near infrared and visible," Prog. Quantum Electron. **26**, 287–352 (2002).
2. M. I. Demchuk, V. P. Mikhailov, N. I. Zhavoronkov, N. V. Kuleshov, P. V. Prokoshin, K. V. Yumashev, M. G. Livshits, and B. I. Minkov, "Chromium-doped forsterite as solid-state saturable absorber," Opt. Lett. **17**, 929–930 (1992).
3. H. Eilers, K. R. Hoffman, W. M. Dennis, S. M. Jacobsen, and W. M. Yen, "Saturation of 1.064 μm absorption in $Cr,Ca:Y_3Al_5O_{12}$ crystals," Appl. Phys. Lett. **61**, 2958–2960 (1992).
4. J. J. Zayhowski and C. Dill, "Diode-pumped passively Q-switched picosecond microchip lasers," Opt. Lett. **19**, 1427–1429 (1994).
5. Y. Shimony, Z. Burshtein, and Y. Kalisky, "Cr^{4+}:YAG as passive Q switch and Brewster plate in a pulsed Nd:YAG laser," IEEE J. Quantum Electron. **31**, 1738–1741 (1995).
6. Y.-F. Chen and S. W. Tsai, "Simultaneous Q switching and mode-locking in a diode-pumped Nd:YVO 4-Cr^{4+}:YAG laser," IEEE J. Quantum Electron. **37**, 580–586 (2001).
7. Y. Kalisky, "Cr^{4+}-doped crystals: their use as lasers and passive Q switches," Prog. Quantum Electron. **28**, 249–303 (2004).
8. H. R. Verdun and L. Merkle, "Evidence of excited-state absorption of pump radiation in the Cr:forsterite laser," in *Digest of Advanced Solid-State Lasers* (Optical Society of America, 1991).
9. V. G. Baryshevski, M. V. Korzhik, M. G. Livshitz, A. A. Tarasov, A. E. Kimaev, I. I. Mishkel, M. L. Meilman, B. J. Minkov, and A. P. Shkadarevich, "Properties of forsterite and the performance of forsterite lasers with lasers and flashlamp pumping," in *Digest of Advanced Solid-State Lasers* (Optical Society of America, 1991).
10. K. Spariosu, W. Chen, R. Stultz, and M. Birnbaum, "Dual Q switching and laser action at 1.06 and 1.44 μm in a Nd^{3+}:YAG-Cr^{4+}:YAG oscillator at 300 K," Opt. Lett. **18**, 814–816 (1993).
11. M. I. Demchuk, N. V. Kuleshov, and V. P. Mikhailov, "Saturable absorbers based on impurity and defect centers in crystals," IEEE J. Quantum Electron. **30**, 2120–2126 (1994).
12. A. Sennaroglu, C. R. Pollock, and H. Nathel, "Efficient continuous-wave chromium-doped YAG laser," J. Opt. Soc. Am. B **12**, 930–937 (1995).
13. A. Sennaroglu, "Continuous wave thermal loading in saturable absorbers: theory and experiment," Appl. Opt. **36**, 9528–9535 (1997).
14. A. Sennaroglu and B. Pekerten, "Experimental and numerical investigation of thermal effects in end-pumped Cr^{4+}:forsterite lasers near room temperature," IEEE J. Quantum Electron. **34**, 1996–2005 (1998).
15. Z. Burshtein, P. Blau, Y. Kalisky, Y. Shimony, and M. R. Kokta, "Excited-state absorption studies of Cr^{4+} ions in several garnet host crystals," IEEE J. Quantum Electron. **34**, 292–299 (1998).
16. N. V. Kuleshov, A. V. Podlipensky, V. G. Shcherbitsky, A. A. Lagatsky, and V. P. Mikhailov, "Excited-state absorption in the range of pumping and laser efficiency of Cr^{4+}:fosterite," Opt. Lett. **23**, 1028–1030 (1998).
17. T. Togashi, Y. Nabekawa, T. Sekikawa, and S. Watanabe,

"High-peak power femtosecond Cr:forsterite laser system," Appl. Phys. B: Photophys. Laser Chem. **68**, 169–175 (1999).
18. G. Xiao, J. H. Lim, S. Yang, E. V. Stryland, M. Bass, and L. Weichman, "*Z*-scan measurement of the ground and excited state absorption cross sections of Cr^{4+} in yttrium aluminum garnet," IEEE J. Quantum Electron. **35**, 1086–1091 (1999).
19. A. Suda, A. Kadoi, K. Nagasaka, H. Tashiro, and K. Midorikawa, "Absorption and oscillation characteristics of a pulsed Cr^{4+}:YAG laser investigated by a double-pulse pumping technique," IEEE J. Quantum Electron. **35**, 1548–1553 (1999).
20. A. G. Okhrimchuk and A. V. Shestakov, "Absorption saturation mechanism for YAG:Cr^{4+} crystals," Phys. Rev. B **61**, 988–995 (2000).
21. A. Sennaroglu, "Analysis and optimization of lifetime thermal loading in continuous-wave Cr^{4+}-doped solid-state lasers," J. Opt. Soc. Am. B **18**, 1578–1586 (2001).
22. A. Sennaroglu, A. Kurt, and S. Buhours, "Analysis and optimization of diode end-pumped solid-state lasers: Application to Nd^{3+}:YVO_4 lasers at 1064 and 1342 nm," Opt. Eng. **44**, 054202 (2005).
23. A. Sennaroglu and B. Pekerten, "Determination of the optimum absorption coefficient in Cr^{4+}:forsterite lasers under thermal loading," Opt. Lett. **23**, 361–363 (1998).
24. Y. Kalisky, R. Moncorge, Y. Guyot, and M. Kokta, "Laser operation and *Q*-switching properties of (Cr^{4+},Mg^{2+}):YAG crystal," in *Advanced Solid-State Lasers*, Vol. 19 of OSA Trends in Optics and Photonics Series (Optical Society of America, 1998).
25. S. Kück, K. Petermann, and G. Huber, "Spectroscopic investigation of the Cr^{4+}-center in YAG," in *Advanced Solid-State Lasers* (Optical Society of America, 1991).
26. N. I. Borodin, V. A. Zhitnyuk, A. G. Okhrimchuk, and A. V. Shestakov, "Oscillation of a $Y_3Al_5O_{12}$:Cr^{4+} laser in wave length region of 1.34–1.6 mm," Izv. Akad. Nauk SSSR Ser. Fiz. **54**, 1500–1506 (1990).
27. S. Naumov, E. Sorokin, and I. T. Sorokina, "Measurement of the excited state absorption cross-section in Cr^{4+}:YAG using relaxation oscillations study," in *Advanced Solid-State Photonics*, Vol. 98 of OSA Trends in Optics and Photonics Series (Optical Society of America, 2005).
28. J. Chen, H.-F. Yau, H.-P. Liu, T.-C. Chen, C.-C. Cheng, and F.-M. Liu, "Passive *Q*-switch and mode-locking modulators for Nd:hosted lasers," Opt. Laser Technol. **32**, 215–219 (2000).
29. T. Dascalu, G. Philipps, and H. Weber, "Investigation of a Cr^{4+}:YAG passive *Q*-switch in cw pumped Nd: YAG lasers," Opt. Laser Technol. **29**, 145–149 (1997).